

RESEARCH ARTICLE

A novel model for treatment of hypertrophic pachymeningitis

Yiwen Cui^{1,a}, Katsuhisa Masaki^{1,a}, Xu Zhang¹, Ryo Yamasaki¹, Takayuki Fujii¹, Hidenori Ogata¹, Shotaro Hayashida¹, Hiroo Yamaguchi¹, Fuminori Hyodo², Hinako Eto², Sachiko Koyama¹, Kyoko Iinuma¹, Tomomi Yonekawa¹, Takuya Matsushita^{1,3}, Mari Yoshida⁴, Kazunori Yamada⁵, Mitsuhiro Kawano⁶, Marie Malissen⁷, Bernard Malissen⁷ & Jun-ichi Kira¹

¹Department of Neurology, Neurological Institute, Graduate School of Medical Sciences, Kyushu University, Fukuoka, Japan

²Innovation Center for Medical Redox Navigation, Kyushu University, Fukuoka, Japan

³Department of Neurological Therapeutics, Neurological Institute, Graduate School of Medical Sciences, Kyushu University, Fukuoka, Japan

⁴Department of Neuropathology, Institute for Medical Science of Aging, Aichi Medical University, Nagakute, Aichi, Japan

⁵Department of Advanced Research in Community Medicine, Graduate School of Medical Sciences, Kanazawa University, Kanazawa, Japan

⁶Division of Rheumatology, Department of Internal Medicine, Kanazawa University Graduate School of Medicine, Kanazawa, Japan

⁷Centre d'Immunologie de Marseille-Luminy, Aix Marseille Université, INSERM, CNRS, Marseille 13288, France

Correspondence

Jun-ichi Kira, Department of Neurology, Neurological Institute, Graduate School of Medical Sciences, Kyushu University, 3-1-1 Maidashi, Higashi-ku, Fukuoka 812-8582, Japan. Tel: +81-92-642-5340; Fax: +81-92-642-5352; E-mail: kira@neuro.med.kyushu-u.ac.jp

Funding Information

This study was supported in part by a Health and Labour Sciences Research Grant on Intractable Diseases (H26-Nanchitou (Nan)-Ippan-074) from the Ministry of Health, Labour and Welfare, Japan (J.K.); the Practical Research Project for Rare/Intractable Diseases from the Japan Agency for Medical Research and Development (AMED) (J.K.); a "Glial assembly" Grant-in-Aid for Scientific Research on Innovative Areas (MEXT KAKENHI Grant Numbers 25117001 and 25117012) from the Ministry of Education, Culture, Sports, Science and Technology of Japan (J.K.); JSPS KAKENHI Grants-in-Aid for Scientific Research (A) (Grant Number 16H02657) (J.K.), (C) (Grant Number 16K09694) (R.Y.), and (C) (Grant Number 26461295) (K.M.) from the Japan Society for the Promotion of Science, and CNRS and INSERM (B.M. and M.M.).

Received: 21 October 2018; Accepted: 5 December 2018

Annals of Clinical and Translational Neurology 2019; 6(3): 431–444

doi: 10.1002/acn3.715

^aThese authors contributed equally to this work.

Abstract

Objective: Immunoglobulin (Ig)G4-related disease is a major cause of hypertrophic pachymeningitis (HP), presenting as a progressive thickening of the dura mater. HP lacks an animal model to determine its underlying mechanisms. We developed a suitable animal model for the treatment of HP. **Methods:** We longitudinally evaluated dura in mice with a mutation (Y136F) in the linker for activation of T cells (LAT), which induced type 2 T helper (Th2) cell proliferation and IgG1 (IgG4 human equivalent) overexpression. Mice were therapeutically administered daily oral irbesartan from 3 to 6 weeks of age. Human IgG4-related, anti-neutrophil cytoplasmic antibody-related, and idiopathic HP dura were also immunohistochemically examined. **Results:** LATY136F mice showing dural gadolinium enhancement on magnetic resonance imaging had massive infiltration of B220⁺ B cells, IgG1⁺ cells, CD138⁺ plasma cells, CD3⁺ T cells, F4/80⁺ macrophages, and polymorphonuclear leukocytes in the dura at 3 weeks of age, followed by marked fibrotic thickening. In dural lesions, transforming growth factor (TGF)- β 1 was produced preferentially in B cells and macrophages while TGF- β receptor I (TGF- β RI) was markedly upregulated on fibroblasts. Quantitative western blotting revealed significant upregulation of TGF- β 1, TGF- β RI, and phosphorylated SMAD2/SMAD3 in dura of LATY136F mice aged 13 weeks. A similar upregulation of TGF- β RI, SMAD2/SMAD3, and phosphorylated SMAD2/SMAD3 was present in autopsied dura of all three types of human HP. Irbesartan abolished dural inflammatory cell infiltration and fibrotic thickening in all treated LATY136F mice with reduced TGF- β 1 and nonphosphorylated and phosphorylated SMAD2/SMAD3. **Interpretation:** TGF- β 1/SMAD2/SMAD3 pathway is critical in HP and is a potential novel therapeutic target.

Introduction

Hypertrophic pachymeningitis (HP) is an intractable neurologic disease that causes inflammatory fibrous thickening of the brain and spinal dura.^{1,2} Although corticosteroids and immunosuppressants are used to treat HP, it is frequently resistant to immunotherapies, resulting in serious sequelae.^{3–5} Because no relevant animal model of HP currently exists, there is an urgent need to develop an appropriate animal model to investigate the disease pathogenesis of HP.

We previously conducted a nationwide survey of HP in Japan and identified two major causes: immunoglobulin (Ig)G4-related and anti-neutrophil cytoplasmic antibody (ANCA)-related disease.⁶ IgG4-related disease is an increasingly recognized disease presenting with a lymphoplasmacytic infiltrate enriched for IgG4-positive plasma cells in multiple organs,⁷ which undergo progressive fibrosis.^{8,9} Type 2 T helper (Th2) cells play a key role in this condition because IgG4 production is driven by Th2 cytokines.^{7–9}

In the present study, we established a novel animal model of HP using IgG4-related disease model mice¹⁰ with a mutation (Y136F) in the linker for activation of T cells (LAT) to investigate therapeutic targets.^{11–13} LAT controls the development and function of T cells by assembling a multiprotein complex following tyrosine phosphorylation.^{11–13} LATY136F mutant mice, in which tyrosine at position 136 of LAT is replaced with phenylalanine, develop an early proliferation of Th2 cells that produce large amounts of Th2 cytokines, leading to hyper-IgG1 (IgG4 human equivalent) and hyper-IgEaemia.^{11–13} Here, we report inflammatory fibrosis of the dura mater of LATY136F mutant mice with a marked upregulation of the transforming growth factor- β (TGF- β)/SMAD pathway, which was effectively treated with irbesartan, an angiotensin II receptor type I (AT1) blocker, which suppressed TGF- β signaling.

Materials and Methods

Human subjects

Autopsied dura specimens of patients with IgG4-related HP,¹⁴ myeloperoxidase (MPO)-ANCA-related HP, idiopathic HP, and cerebral infarction were obtained from the Department of Neuropathology, Institute for Medical Science of Aging, Aichi Medical University (Aichi, Japan) (Table S1). This study involving the analysis of consenting human subjects was approved by The Kyushu University Institutional Review Board for Clinical Research.

Mice

Transgenic offspring of LATY136F mutant mice were genotyped by polymerase chain reaction (PCR) using DNA

obtained from ear biopsies. The primer pair for PCR amplification was LATY136F D (5'-GTGGCAAGCTACGAGAAC-CAGGGT-3' and LATY136F U (5'-GACGAAGGAGCAAAGGTGGAAGGA-3'). This study was approved by the Recombinant DNA Experiment Safety Committee of the Graduate School of Medical Sciences, Kyushu University. Animals were handled consistent with the guidelines for the care and use of laboratory animals of our institution.

Pathological analysis

The brain plus skull and the cervical spinal cord plus spinal column were placed in Plank-Rychlo Solution (Muto Pure Chemicals, Co. Ltd., Tokyo, Japan) for decalcification at 4°C overnight. The tissues were fixed in 10% buffered formalin and processed into paraffin sections (5 μ m thick). All sections underwent hematoxylin and eosin (HE) and Masson's trichrome (MT) staining. For immunohistochemistry, deparaffinized sections were hydrated in ethanol and then incubated with 0.3% hydrogen peroxide in absolute methanol for 30 min. The sections were incubated with a primary antibody (Table S2) at 4°C overnight. After rinsing, sections were subjected to labeling with the Envision system (DakoCytomation, Glostrup, Denmark).

Indirect immunofluorescence and confocal laser microscopy

All sections were deparaffinized in xylene and rehydrated through an ethanol gradient. Sections were then incubated with primary antibodies at 4°C overnight. After rinsing, sections were incubated with Alexa 488-conjugated goat anti-mouse IgG and Alexa 546-conjugated goat anti-rabbit IgG (Invitrogen, Carlsbad, CA), and then counterstained with DAPI. Images were captured using a confocal laser microscope system (Nikon A1, Nikon, Tokyo, Japan).

Evaluation of lesion distribution in dural tissues

Brains plus skulls were sliced into coronal sections and examined at five levels: frontal lobe, corpus callosum, hippocampus, brainstem, and cerebellum. The pathology of dura mater around the superior sagittal sinus (SSS) and that of the calvaria at each level were analyzed. The extent of lesions was determined by assessing the inflammatory infiltrates and thickening of the dura at each level of tissue stained with HE. Inflammatory cells infiltrating the dura mater limited to an area around the SSS were termed "DM-S" lesions, while lesions affecting both the dura mater around the SSS area and toward the calvaria from the SSS were termed "DM-C".

Quantification of inflammatory cells and thickening of the dura mater

The sections used for immunostaining and HE staining were also used for manual counting of the absolute number of infiltrating inflammatory cells, including CD3⁺ T cells, B220⁺ B cells, CD138⁺ plasma cells, F4/80⁺ macrophages, IgG1-positive cells, and polymorphonuclear leukocytes in dural lesions of DM-S and DM-C in LATY136F mutant mice. We also manually counted the absolute number of CD3⁺ T cells, B220⁺ B cells, and F4/80⁺ macrophages merged with TGF- β 1 or phosphorylated SMAD2/SMAD3 staining. To assess the thickening of the cranial dura mater and the cervical spinal cord dura, areas of thickened dura mater from LATY136F mutant and WT mice were calculated using ImageJ/Fiji at the same magnification (10 \times objective) and values are presented as mm².

Grading fibrotic thickening of the dura

Paraffin sections stained with HE or Masson's trichrome stain were systematically scanned at the same magnification using a microscope (10 \times objective). Each successive field was individually assessed for dural fibrosis thickness and allotted a score from 0 to 3 using the following predetermined scale of severity: grade 0, no fibrosis of the dura (thickness < 10 μ m); grade 1, mild fibrosis of the dura (thickness < 10–50 μ m); grade 2, moderate fibrosis of the dura (thickness < 50–100 μ m); and grade 3, severe fibrosis of the dura (thickness > 100 μ m).

Western blotting

Dura mater of mice ($N = 5$ LATY136 mutant mice and $N = 5$ WT mice) were collected in lysis matrix D tubes (MP Biomedicals, Solon, OH) and immersed in a mixture of radioimmunoprecipitation assay buffer and 0.5% sodium dodecyl sulfate. Thirty micrograms of tissue was subjected to electrophoresis in a 4%–15% Mini-PROTEAN TGX gel (Bio-Rad, Hercules, CA) and blotted onto a polyvinylidene difluoride membrane. After blotting, membranes were incubated in 5% skim milk or Blocking One-P (Nacalai Tesque, Kyoto, Japan). After washing, the membrane was incubated with primary antibodies (Table S3) overnight at 4°C. Membranes were incubated with horseradish peroxidase-conjugated secondary antibodies and then visualized by enhanced chemiluminescence (ECL Western Blotting Detection Reagents, GE Healthcare Bio-Sciences AB, Uppsala, Sweden).

MRI analysis

Brain MRI was performed using a 1.5 T MR VivoLVA scanner (DS Pharma Biomedical Co. Ltd., Osaka, Japan), and 1-mm-thick slices were obtained. Mice were anesthetized by 2.5% isoflurane and subsequently administered 200 μ L of 20 mmol/L gadolinium-diethylenetriamine penta-acetic acid (Gd-DTPA) (Magnevist; Bayer, Leverkusen, Germany) through the tail vein. After 2 min, Gd-DTPA-enhanced T1-weighted images were obtained. For the quantitative analysis of Gd-enhanced lesions, an area measuring 2 \times 6 pixels was defined as the region of interest (ROI) within a Gd-enhanced lesion. The mean intensity change for each pixel (x) was then calculated as follows: $x = [(intensity\ of\ contrast\ enhanced\ image - intensity\ of\ precontrast\ enhanced\ image) / intensity\ of\ precontrast\ enhanced\ image] \times 100$. The mean values for the change in intensity were calculated for each mouse.

Irbesartan treatment

LATY136F mutant mice aged 3 weeks ($N = 6$ LATY136 mutant mice and $N = 5$ WT mice) were orally administered PBS as a placebo or 50 mg/kg per day of irbesartan (Wako Pure Chemical Industries Ltd., Osaka, Japan) for three consecutive weeks, based on a previous report.¹⁵ These mice were sacrificed at 6 weeks of age.

Statistical analysis

JMP pro software (ver. 11.0.0; SAS Institute Japan, Tokyo, Japan) and Prism software (GraphPad 6.0, La Jolla, CA) were used to conduct statistical analyses. All data are expressed as the mean \pm standard deviation (S.D.). Differences in the frequency of inflammatory foci in dura between WT and LATY136F mutant mice were examined for significance using Fisher's exact probability test. The statistical significance of the differences among three or more groups was determined using one-way ANOVA followed by a post hoc multiple-comparisons test (Tukey's). Values of $P < 0.05$ were considered statistically significant.

Results

Identification of dural inflammation and fibrosis in LATY136F mutant mice

Three-week-old LATY136F mutant mice displayed the spontaneous infiltration of immune cells in the cranial dura mater, followed by a marked thickening of the

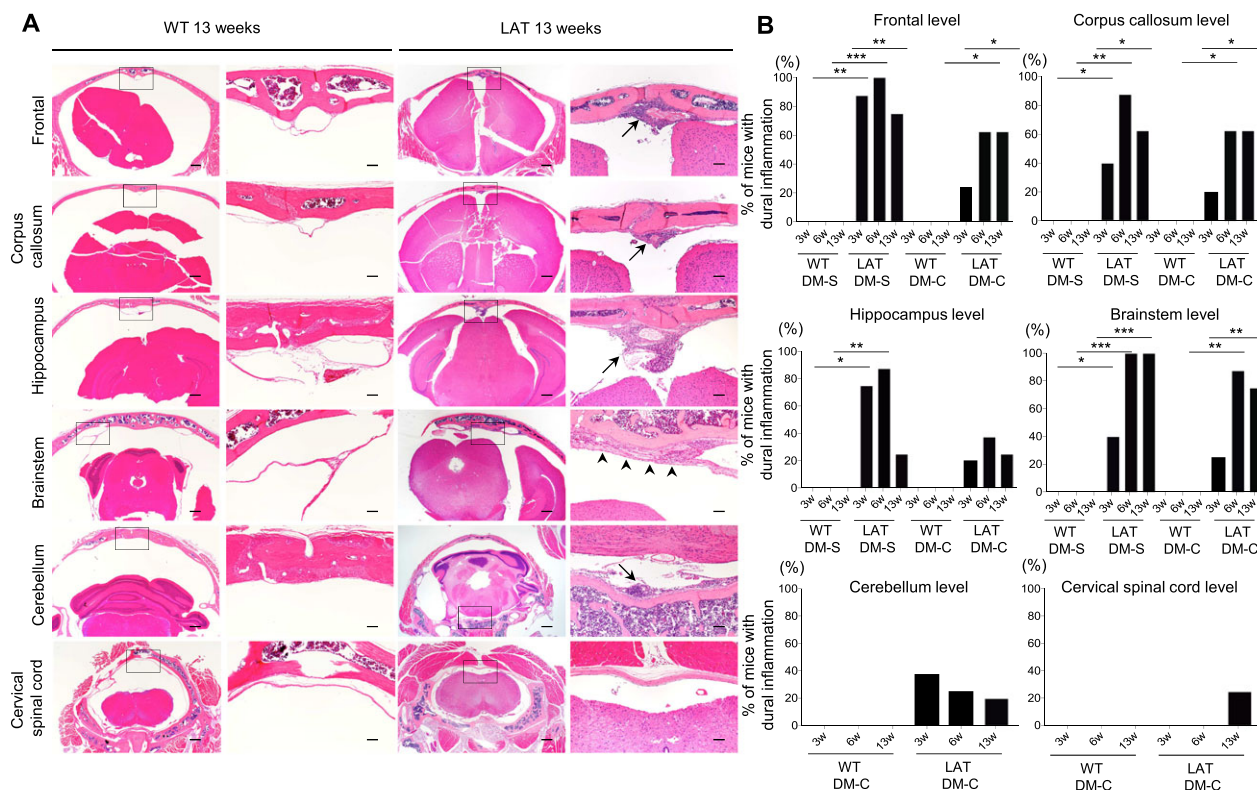


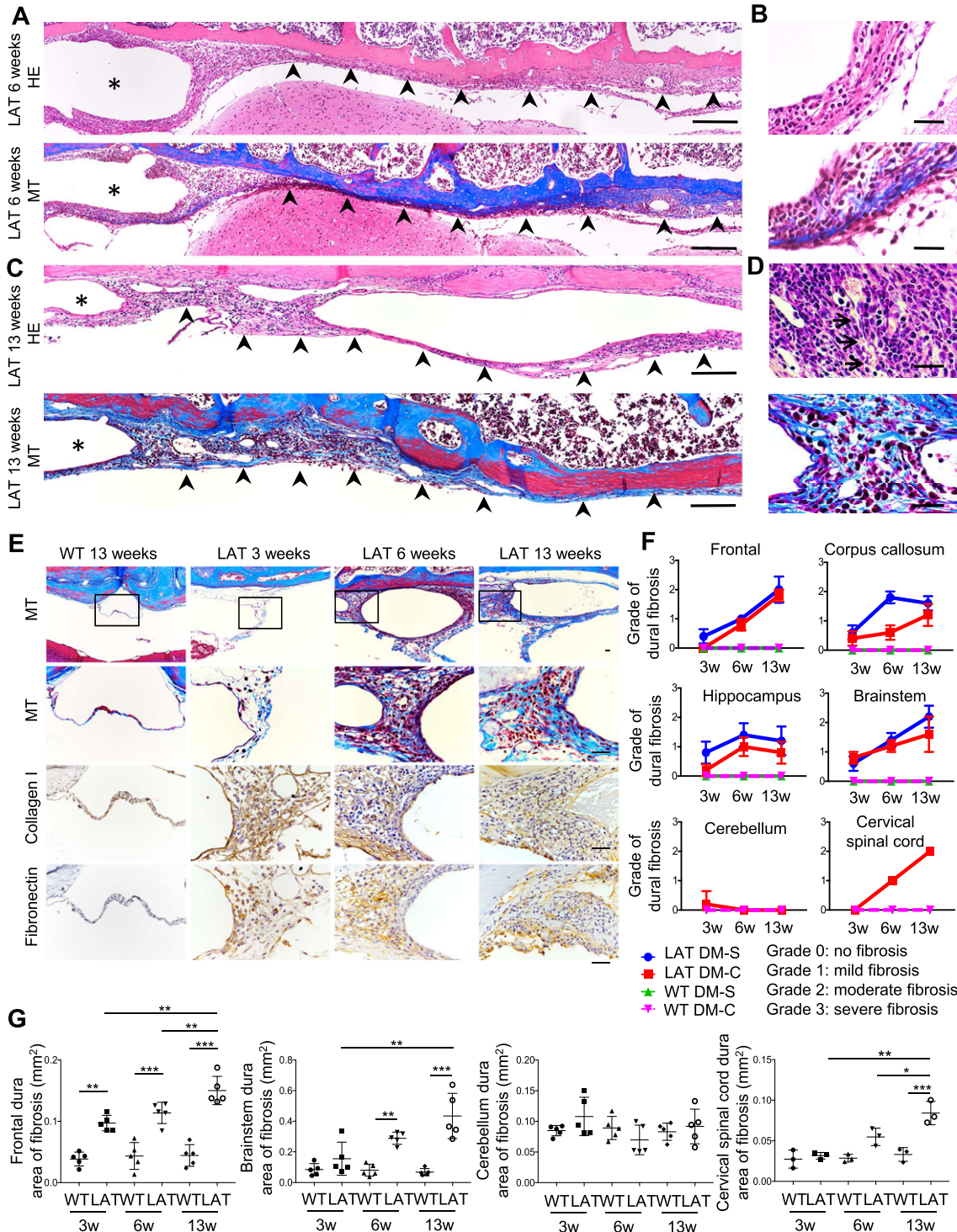
Figure 1. Lesion distribution in the dura of LATY136F homozygous mutant mice. (A) Hematoxylin and eosin (HE) staining of tissues from wild-type (WT) and LATY136F mutant mice aged 13 weeks. In LATY136F mutant mice, infiltrated inflammatory cells were distributed in the dura mater around the superior sagittal sinus (SSS) at the frontal, corpus callosum, hippocampal, and brainstem levels in LATY136F mutant mice (arrows). At the brainstem level, inflammatory cells extended toward the calvaria from the SSS (arrowheads). Scale bars, 500 μ m (low magnification column); 100 μ m (high-magnification column). (B) Frequency of inflammatory cell infiltrates in the dura mater around the SSS (DM-S) and toward the calvaria from the SSS (DM-C) in each cranial region level. The presence or absence of accumulated inflammatory cells (inflammatory foci, arrows in Fig. 1A) at DM-S or DM-C was evaluated by HE staining. The percentage indicates the ratio of the number of mice with dural inflammation in each region level of WT and LATY136F mutant mice ($N = 8$ LATY136 mutant mice and $N = 8$ WT mice). P values calculated by Fisher's exact probability test. * $P < 0.05$, ** $P < 0.01$, *** $P < 0.001$.

dura (Fig. S1). Such inflammatory changes in LATY136F mice were prominent in the dura around the SSS (DM-S) and extended toward the calvaria over the frontal and posterior cranial regions (DM-C) (Fig. 1A and B). Inflammatory infiltrates accumulated focally around the SSS and persisted until 13 weeks of

Figure 2. Fibrotic changes in the dura mater of LATY136F mice. (A) Hematoxylin and eosin (HE) and Masson's trichrome (MT) staining of dural lesions in LATY136F mutant mice aged 6 weeks. Inflammatory lesions with mild fibrotic changes are visible in the dura mater around the SSS as well as extending toward the calvaria from the SSS (arrowheads, DM-C). No inflammatory changes are present in the cerebral parenchyma adjacent to dural lesions. Asterisk indicates SSS. Scale bars, 100 μ m. (B) High-magnification view of a dural lesion shown in Panel A. HE staining shows inflammatory cells including mononuclear and polymorphonuclear cells. MT staining detected reticular collagenous fibers shown as blue in this lesion. Scale bars, 20 μ m. (C) HE and MT staining of dural lesions in LATY136F mutant mice aged 13 weeks. Inflammatory lesions with dense fibrotic changes are present in the dura mater as DM-C (arrowheads). Scale bars, 100 μ m. (D) Storiform fibrosis and obliterative phlebitis in dural lesions of LATY136F mutant mice aged 13 weeks. HE staining shows severe dural vein stenosis associated with massive inflammatory infiltrates. This venous lumen is identified by the existence of erythrocytes (arrows). MT staining shows distinctive fibrosis with an irregular whorled or star-like pattern (storiform fibrosis). Scale bars, 20 μ m. (E) MT staining demonstrates fibrotic changes and thickening of the inflamed dura mater in LATY136F mutant mice aged 3, 6, and 13 weeks. Immunostaining of collagen type I and fibronectin shows a dense deposition of these molecules in the affected dural areas. Panels in the second to fourth rows show higher magnification of the black-boxed areas in the first row. Scale bars 100 μ m (top rows); 20 μ m (other panels). (F) Grading of the fibrous dural thickening at 3, 6, and 13 weeks of age in LATY136F mutant and wild-type (WT) mice. (G) Areas of dural fibrosis determined by Masson's trichrome stain in LATY136F mutant mice increased with age. Fibrotic areas were calculated using ImageJ/Fiji software ($N = 5$ LATY136 mutant mice and $N = 5$ WT mice). P values calculated by Tukey's post hoc test after one-way ANOVA. ** $P < 0.01$, *** $P < 0.001$.

age while dura over the cerebellum and the cervical spinal cord showed only minor inflammation (Fig. 1A and B). Furthermore, fibrotic changes in the cranial dura appeared in inflammatory lesions around the DM-S at 3 weeks of age and extended to the DM-C at

6 weeks of age, where the fibrotic thickening grades of the dura became more severe with increased age (Fig. 2A–F). Moreover, storiform fibrosis and obliterative phlebitis, characteristic of IgG4-related HP,¹⁶ were observed at 13 weeks of age (Fig. 2D). Fibrotic areas in the cranial



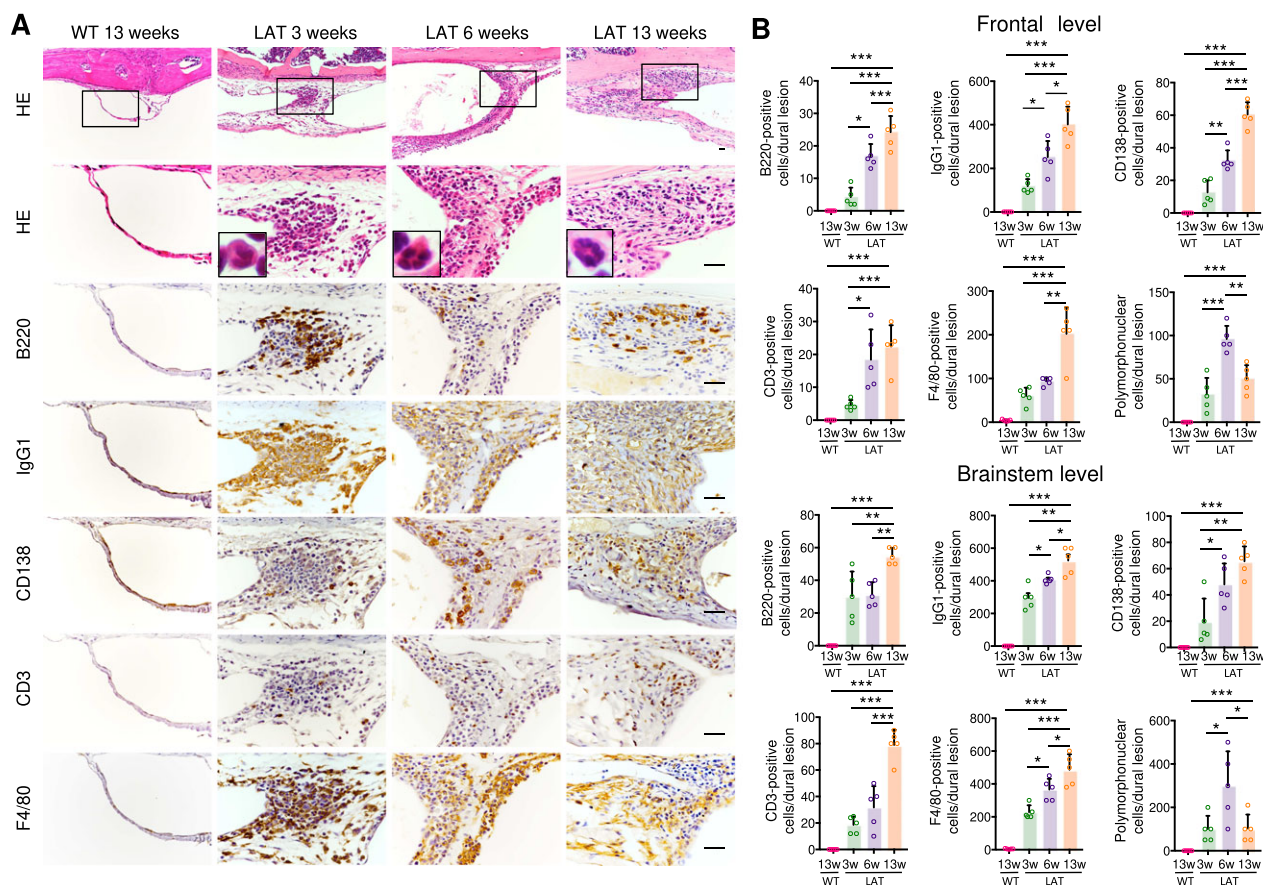


Figure 3. Characterization of infiltrated inflammatory cells in the dura mater. (A) Hematoxylin and eosin (HE) staining and immunostaining in dural lesions of wild-type (WT) mice at 13 weeks of age and LATY136F mutant mice at 3, 6, and 13 weeks of age. Panels in the second row show higher magnification of the black-boxed areas in the first row. HE staining indicates large amounts of inflammatory infiltrates containing mononuclear and polymorphonuclear cells (second row, insets) in the dura mater of LATY136F mutant mice. Immunostaining demonstrates that mononuclear cells consist of B220⁺ B cells, CD138⁺ plasma cells, CD3⁺ T cells and F4/80⁺ macrophages. Immunoreactivity for IgG1 is robustly positive in infiltrated immune cells. Scale bars 20 μ m. (B) The number of infiltrated inflammatory cells in the dura mater of WT mice aged 13 weeks and LATY136F mutant mice aged 3, 6, and 13 weeks. Mean numbers + S.D. of infiltrated inflammatory cells in DM-5 and DM-C at frontal and brainstem levels are expressed as bars, while open circles represent the absolute number in individual mice ($N = 5$ LATY136 mutant mice and $N = 5$ WT mice). P values calculated by Tukey's post hoc test after one-way ANOVA. * $P < 0.05$, ** $P < 0.01$, *** $P < 0.001$.

dura were significantly larger in LATY136F mice than in WT mice (Frontal level, $P < 0.05$ at 3, 6, and 13 weeks of age; Brainstem level, $P < 0.05$ at 6 and 13 weeks of age) (Fig. 2G). The fibrotic areas of the cranial dura in LATY136F mutant mice were significantly increased in an age-dependent manner compared with controls (Fig. 2G). In affected dura with prominent fibrotic changes, collagen type I, and fibronectin were densely deposited as assessed by immunostaining (Fig. 2E). In addition, dura at the cervical spinal cord also showed fibrotic thickening with increased age, which was significantly more prominent in LATY136F mice than in WT mice at later stages ($P < 0.05$ at 13 weeks of age) (Fig. 2G).

Profile of inflammatory infiltrates in dural lesions of LATY136F mutant mice

Immunostaining analyses demonstrated that B220⁺ B cells and IgG1⁺ cells focally infiltrated the dura near the SSS at 3 weeks of age in LATY136F mutant mice (Fig. 3A). B220⁺ B cells, IgG1⁺ cells, CD138⁺ plasma cells, CD3⁺ T cells, and F4/80⁺ macrophages abundantly infiltrated the inflammatory lesions of the dura at 3, 6, and 13 weeks of age in all LATY136F mutant mice examined. The numbers of infiltrated inflammatory cells were significantly increased with age at both the frontal and brainstem levels (Fig. 3B). The number of polymorphonuclear

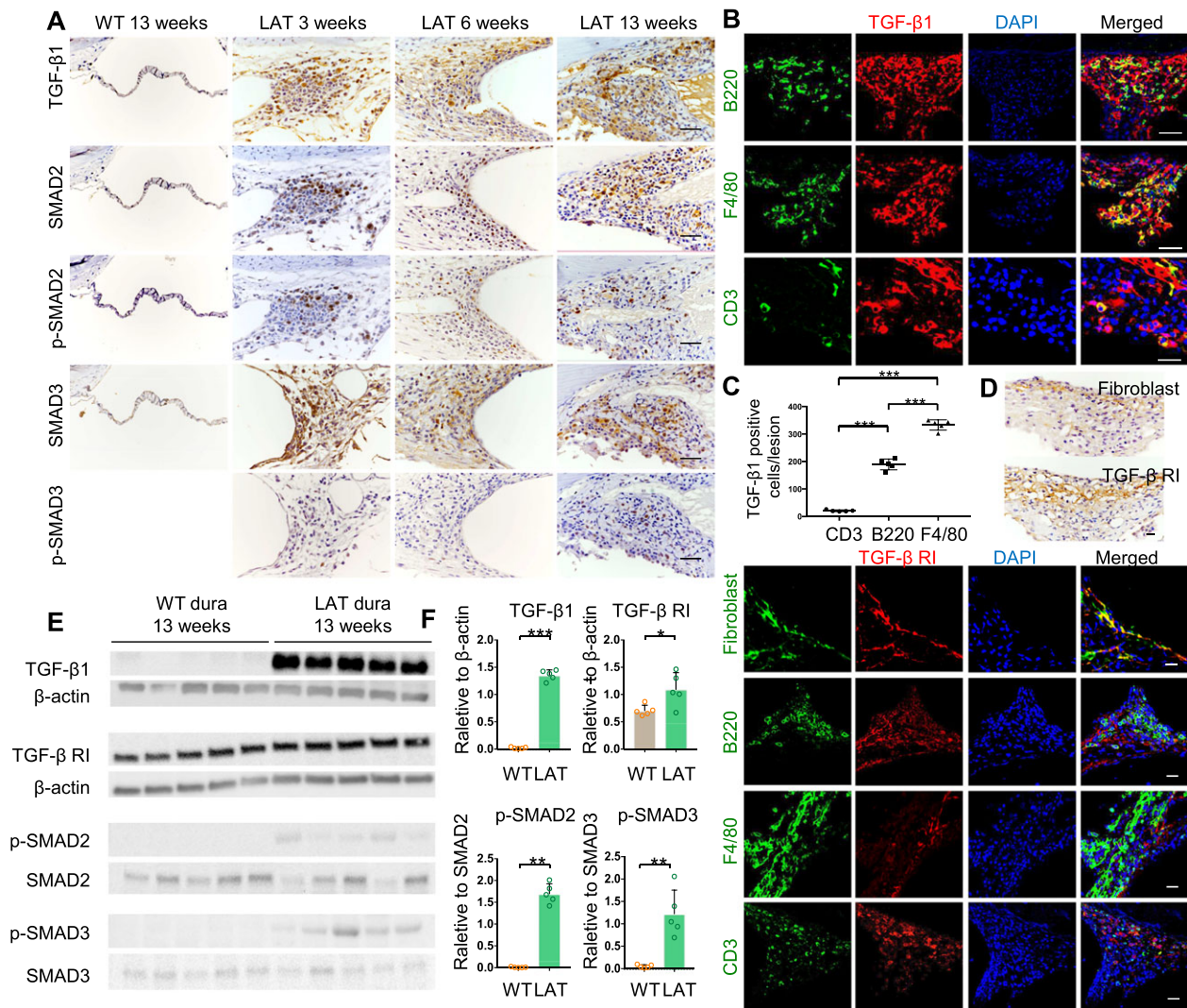


Figure 4. Upregulation of TGF- β /SMAD signaling in LATY136F mice. (A) Expressions of TGF- β 1, and non-phosphorylated and phosphorylated SMAD2/SMAD3 in the inflamed dura mater of LATY136F mutant mice aged 3, 6, and 13 weeks. The panels are a higher magnification of the black-boxed areas in the first row of Fig. 3E. Scale bars, 20 μ m. (B) Expression of TGF- β 1 is colocalized with B220⁺ B cells, F4/80⁺ macrophages, and low numbers of CD3⁺ T cells in inflammatory lesions of the dura in LATY136F mutant mice aged 6 weeks. Scale bars, 50 μ m (top and middle rows); 10 μ m (bottom row). (C) Frequency of TGF- β 1-positive cells in the dural lesions of LATY136F mutant mice aged 6 weeks ($N = 5$ LATY136 mutant mice and $N = 5$ WT mice). Expression of TGF- β 1 was significant and highest in F4/80⁺ macrophages, followed by B220⁺ B cells. (D) Upper panels show single immunostaining of fibroblasts and TGF- β receptor I (TGF- β RI) with a similar staining pattern to the dural lesions of 6-week-old LATY136F mutant mice. Lower panels show double immunostaining of fibroblasts, B220⁺ B cells, F4/80⁺ macrophages, CD3⁺ T cells and TGF- β RI in the dural lesions of 6-week-old LATY136F mutant mice. TGF- β RI is predominantly expressed in fibroblasts. Scale bars, 10 μ m. (E, F) Quantitative western blot analysis of TGF- β /SMAD2/SMAD3 signaling in the dura of LATY136F mutant mice. (E) Representative images of TGF- β 1, TGF- β RI, p-SMAD2 and p-SMAD3 immunoblots obtained from wild-type (WT) mice and LATY136F mutant mice at 13 weeks of age ($N = 5$ LATY136 mutant mice and $N = 5$ WT mice). β -actin and SMAD2/SMAD3 blots for loading controls are shown under each protein blot. (F) Results of quantitative analysis for each protein. The expression levels of TGF- β 1 and TGF- β RI are significantly increased in the dura of LATY136F mutant mice compared with WT mice. In addition, phosphorylated SMAD2 and SMAD3 are significantly increased in the dura of LATY136F mutant mice. P values calculated by Tukey's post hoc test after one-way ANOVA. * $P < 0.05$, ** $P < 0.01$, *** $P < 0.001$.

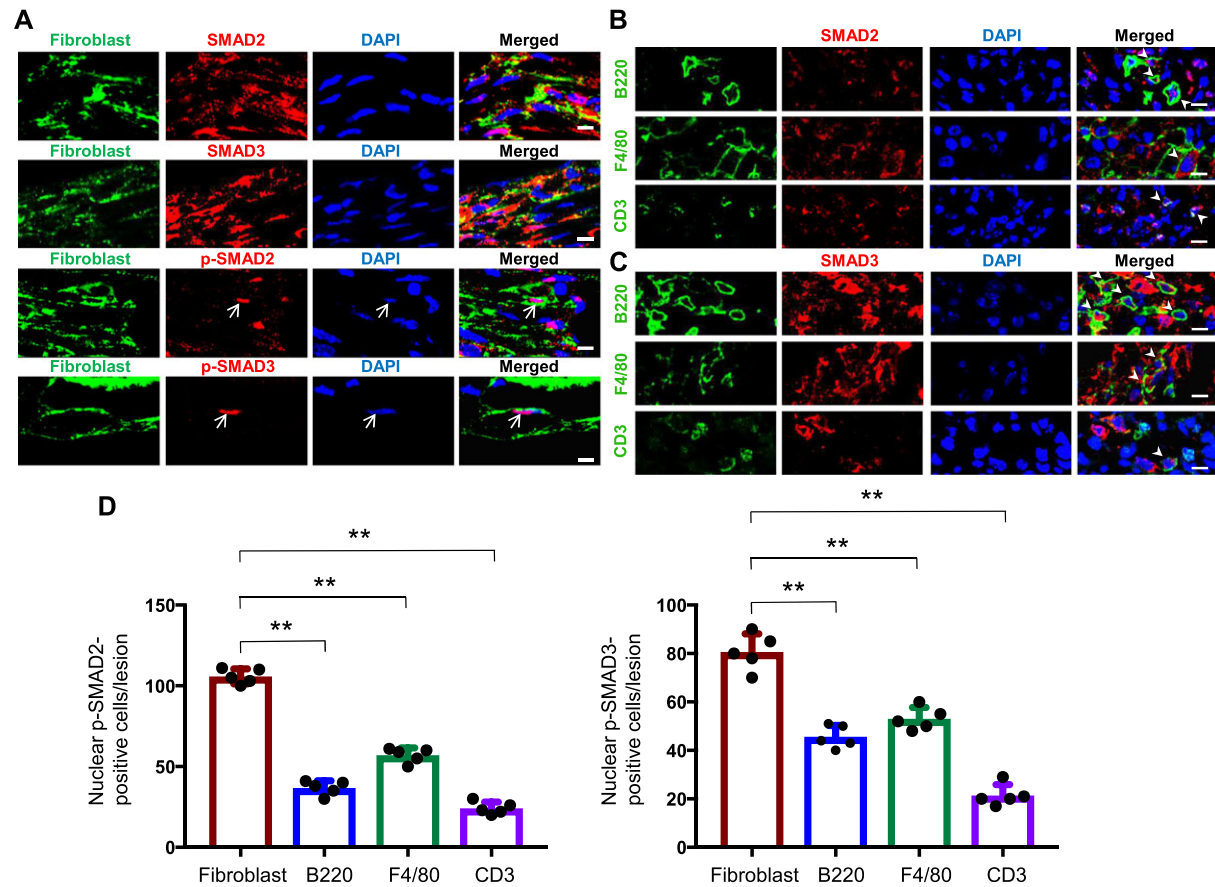


Figure 5. Expression of non-phosphorylated and phosphorylated SMAD2/SMAD3 in fibroblasts in the dural lesions of LATY136F mutant mice. (A) Double immunofluorescence staining for reticular fibroblasts (green) and non-phosphorylated SMAD2 and SMAD3 (red) in the dural lesions of LATY136F mutant mice aged 6 weeks. Non-phosphorylated SMAD2 and SMAD3 are predominantly expressed in the cytoplasm, while phosphorylated SMAD2 and SMAD3 are mainly localized in the nuclei of fibroblasts (arrows). Fibroblast nuclei (DAPI, blue) have an elongated shape, which differs from infiltrated inflammatory cells. Scale bars, 10 μ m. (B, C) Double immunofluorescence staining of infiltrated B220⁺ B cells, F4/80⁺ macrophages or CD3⁺ T cells (green) with non-phosphorylated SMAD2 or SMAD3 (red) in the dural lesions of LATY136F mutant mice aged 6 weeks. Non-phosphorylated SMAD2/SMAD3 are expressed in the cytoplasm of B220⁺ B cells, F4/80⁺ macrophages and CD3⁺ T cells (arrows). Scale bars, 10 μ m. (D) Frequency of the nuclear staining of phosphorylated SMAD2 and SMAD3 in the dural lesions of LATY136F mutant mice aged 6 weeks ($N = 5$ LATY136 mutant mice and $N = 5$ WT mice). Nuclear phosphorylated SMAD2 and SMAD3 were significantly higher in fibroblasts than in B220⁺ B cells, F4/80⁺ macrophages and CD3⁺ T cells. P values calculated by Tukey's post hoc test after one-way ANOVA. ** $P < 0.01$.

in the dura of LATY136F mutant mice peaked at 6 weeks of age and then decreased at 13 weeks of age (Fig. 3B).

Upregulation of TGF- β /SMAD signaling in the dural lesions of LATY136F mutant mice

Immunoreactivity for TGF- β 1 was markedly upregulated and phosphorylated SMAD2 and SMAD3 were abundantly present in the dural lesions of LATY136F mice but not in WT mice (Fig. 4A). Double immunostaining revealed that TGF- β 1 was most frequently expressed in F4/80⁺ macrophages, followed by B220⁺ B cells, but in few CD3⁺ T cells (Fig. 4B and C). By contrast, TGF-

β RI was predominantly expressed on fibroblasts, but not on other inflammatory cells such as B220⁺ B cells, F4/80⁺ macrophages or CD3⁺ T cells in inflamed dural lesions (Fig. 4D). Quantitative western blotting analysis also demonstrated the upregulation of TGF- β 1 ($P < 0.0001$) and TGF- β RI ($P = 0.041$), and the phosphorylation of SMAD2 ($P = 0.004$) and SMAD3 ($P = 0.009$) in the dura of LATY136F mutant mice but not in WT mice at 13 weeks of age (Fig. 4E and F). Nuclear staining of phosphorylated SMAD2 and SMAD3 was significantly more frequent in fibroblasts than in B220⁺ B cells, F4/80⁺ macrophages and CD3⁺ T cells (Fig. 5A–D).

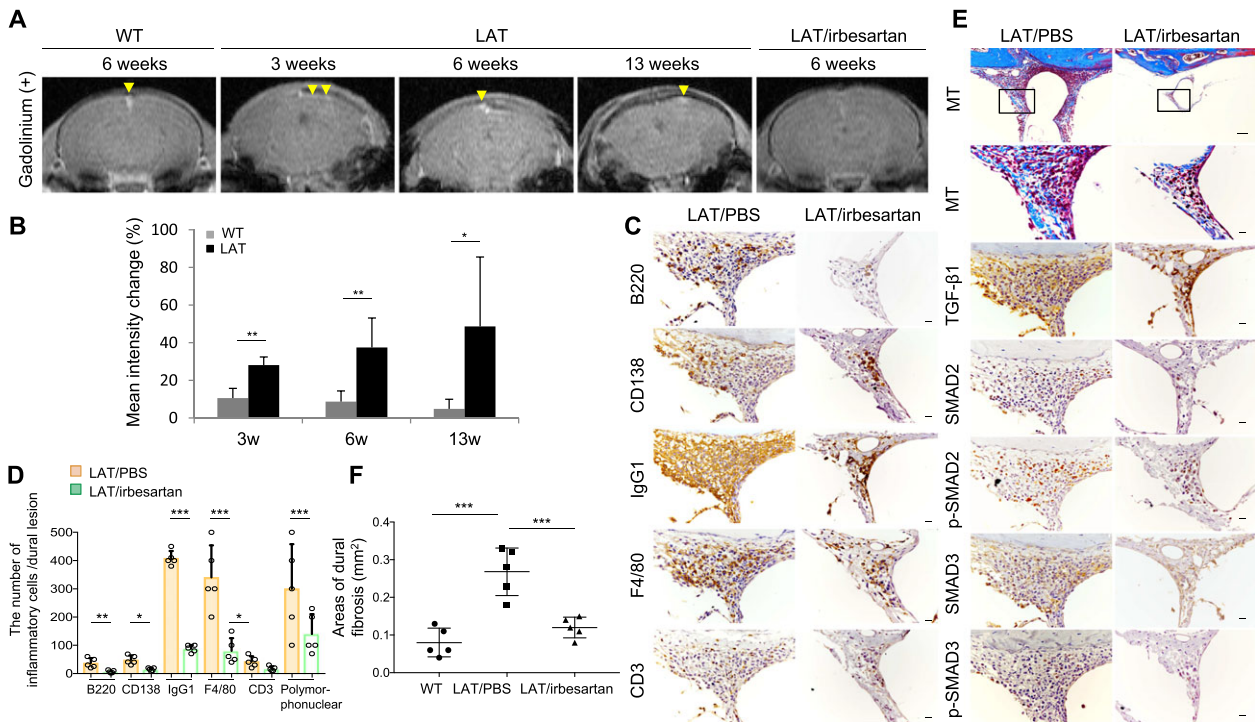


Figure 6. Detection of dural lesions by MRI and treatment effects of irbesartan on dural inflammation and fibrosis in LATY136F mutant mice. (A) Coronal T1-weighted MR images with pre- or post-Gd-DTPA administration. Focal enhancement of the dura is seen on postcontrast images (arrowheads). The imaging parameters for the brain MRI are as follows: T1-weighted gradient echo imaging using a repetition time/echo time of 100/6 msec; field-of-view, 32 × 32 mm; matrix, 128 × 256; accumulations, 8. (B) Quantification of dural enhancement. Mean rates of intensity changes in regions of interest between pre- and post-Gd-DTPA administration ($N = 5$ LATY136 mutant mice and $N = 5$ WT mice). (C) Immunostaining of inflammatory cell markers in the dural lesions of LATY136F mutant mice treated with irbesartan or phosphate-buffered saline (PBS). Scale bars, 10 μ m. (D) Infiltrated inflammatory cell number in the dura mater of irbesartan- or PBS-treated LATY136F mutant mice. Mean number of infiltrated inflammatory cells in DM-S and DM-C at the brainstem level is expressed as bars, and open circles represent the absolute number in an individual mouse ($N = 5$ LATY136 mutant mice and $N = 5$ WT mice). (E) Masson's trichrome (MT) stain and immunostaining of dural fibrosis in LATY136F mutant mice treated with irbesartan or PBS. Scale bars, 100 μ m (top row); 10 μ m (other panels). Panels in the second to sixth rows show a higher magnification of the black-boxed areas in the first row. (F) Area of dural fibrosis at the brainstem level in irbesartan- or PBS-treated LATY136F mutant mice and WT mice ($N = 5$ LATY136 mutant mice and $N = 5$ WT mice). Although LATY136F mutant mice displayed normal peripheral lymphoid organs at birth, their spleen and lymph nodes started to enlarge at 3 weeks of age compared with WT or heterozygous mutant mice.^{11–13} Microscopically, various immune cells, including lymphocytes, macrophages, polymorphonuclear cells, and IgG1⁺ cells abundantly infiltrated around the blood vessels of these organs and fibrotic changes with dense collagen deposition also occurred at 6 and 13 weeks (data not shown). Irbesartan administration suppressed the enlargement of the spleen, liver, and lungs, where perivascular inflammatory infiltrates and fibrotic changes were markedly diminished (data not shown). No fibrotic changes were observed in these organs of WT mice aged 13 weeks. * $P < 0.05$, ** $P < 0.01$, *** $P < 0.001$ (Tukey's post hoc test after one-way ANOVA).

Detection of active dural inflammation in LATY136F mutant mice by MRI

Longitudinal MRI studies showed that the dura mater had focal curvilinear contrast enhancement around the SSS and scattered enhancement over the frontal, temporal, parietal, and occipital lobes on Gd-DTPA-enhanced images of LATY136F mutant mice aged 3 weeks (Fig. 6A). Such dural enhancement was identified in all LATY136F mutant mice tested and extended over the cerebrum and cerebellum at 6 and 13 weeks of age (Fig. 6A). The quantitative analysis of enhanced lesions revealed that dural

areas with focal enhancement after Gd-DTPA were significantly larger in LATY136F mice than in WT mice ($P = 0.004$ at 3 weeks of age, $P = 0.0038$ at 6 weeks of age, and $P = 0.03$ at 13 weeks of age) and increased with age only in LATY136F mutant mice (Fig. 6B).

Suppression of dural inflammation and fibrosis in LATY136F mutant mice by the therapeutic administration of irbesartan

We treated LATY136F mutant mice with irbesartan from 3 to 6 weeks of age. Irbesartan administration completely

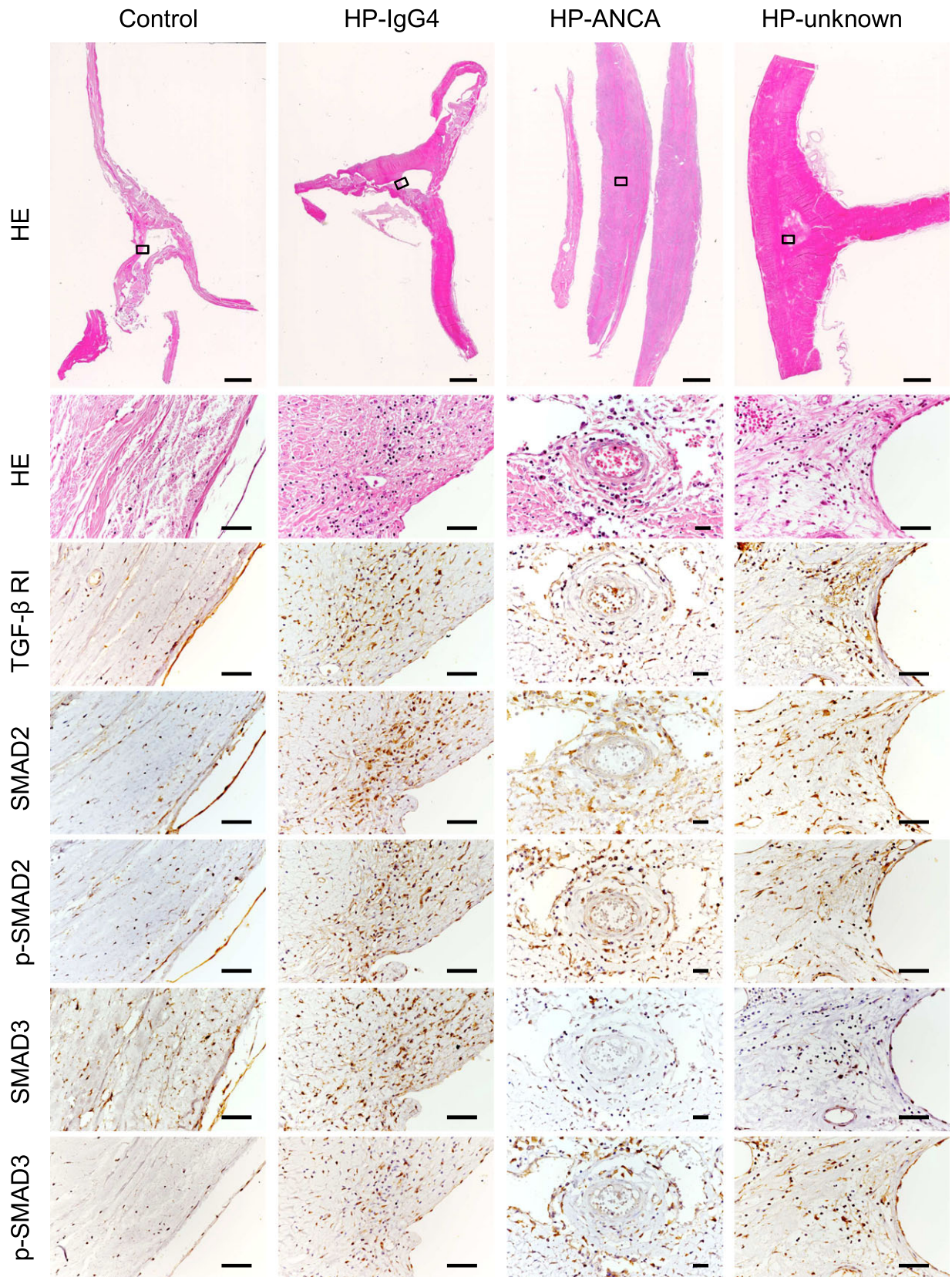


Figure 7. Upregulation of TGF- β /SMAD signaling in the inflamed fibrotic dural lesions of patients with hypertrophic pachymeningitis (HP). Hematoxylin and eosin (HE) staining and immunostaining for TGF- β RI and SMAD2/SMAD3 of dural tissues from patients with IgG4-related HP (HP-IgG4), MPO-ANCA-related HP (HP-ANCA), idiopathic HP (HP-unknown), and cerebral infarction (control case). Panels of the top row show the overview of dura from each autopsied case and other panels show a higher magnification of the squared areas in panels of the top row. In HP-IgG4, diffuse inflammatory cell infiltration and severe interstitial fibrosis are seen. In HP-ANCA, diffuse infiltrates in the dura consist predominantly of lymphocytes, plasma cells, and neutrophils with a thickening of vessel walls indicating vasculitis. Giant cells and severe interstitial fibrosis are also present in this lesion. In HP-unknown, moderate inflammatory infiltrates consisting of lymphocytes and moderate fibrotic changes are visible. Scale bars, 4 mm (top rows); 50 μ m (other panels).

abolished the Gd-DTPA enhancement of the dura mater in all treated LATY136F mutant mice at 6 weeks of age (Fig. 6A). Histologically, irbesartan significantly decreased the number of infiltrated B220⁺ B cells ($P = 0.005$), CD138⁺ plasma cells ($P = 0.0019$), IgG1⁺ cells ($P < 0.0001$), F4/80⁺ macrophages ($P < 0.0001$), CD3⁺ T cells ($P = 0.047$) and polymorphonuclear cells ($P < 0.0001$) in the dural lesions (Fig. 6C, D). The immunoreactivity levels of TGF- β 1 as well as nonphosphorylated and phosphorylated SMAD2/SMAD3 were also diminished (Fig. 6E), and the areas of dural fibrosis were markedly decreased by irbesartan treatment ($P = 0.0006$, Fig. 6F).

Upregulation of TGF- β /SMAD signaling in autopsied tissues from human HP patients

Massive inflammatory cell infiltration and fibrotic changes of the thickened dura were observed in IgG4-related HP (Fig. 7). We found markedly increased immunoreactivities of TGF- β RI, SMAD2, and SMAD3, and phosphorylated SMAD2 and SMAD3 in dural lesions near the SSS in IgG4-related HP (Fig. 7). We then examined the dura mater from autopsied patients with MPO-ANCA-related HP, and idiopathic HP, both of which demonstrated inflammatory infiltrates and fibrotic changes in the dural lesions. Surprisingly, increased immunoreactivities of TGF- β RI, SMAD2, and SMAD3 and phosphorylated SMAD2 and SMAD3 were also detected in the inflamed dural lesions of MPO-ANCA-related HP and idiopathic HP (Fig. 7).

Discussion

The lymphoplasmacytic infiltration of IgG1⁺ (equivalent to human IgG4⁺) cells together with storiform fibrosis and obliterative phlebitis in LATY136F mice suggests that the essential components of human IgG4-related HP are reproduced in this animal model. The more severe involvement of the cranial dura mater rather than the spinal dura mater is also common in human IgG4-related HP and LATY136F mutant mice.⁶ Accordingly, we report that LATY136F mice are a suitable model of human IgG4-related HP. In LATY136F mutant mice,

overproduced Th2 cytokines drive plasma cell differentiation and proliferation with class switching to IgG1 and IgE.^{11–13} The same is true for human IgG4.^{17–19} Therefore, it is likely that Th2 cells play a crucial role in human IgG4-related HP as well as in the LATY136F mutant mouse model.

The robust production of TGF- β 1 in infiltrating B cells and macrophages together with the upregulation of TGF- β RI and phosphorylated SMAD2/SMAD3 in fibroblasts was evident in the afflicted dura of LATY136F mutant mice. Activated B cells play a pathogenic role in tissue fibrosis²⁰ and were reported to produce TGF- β 1 as well as IL-6, which induces Th2-immune responses that increase extracellular matrix deposition during fibrosis. Regarding macrophages, there is growing evidence for a close relationship between macrophages and fibroblasts.²¹ Inflammatory macrophages secrete cytokines and chemokines that activate and recruit fibroblasts. Especially, the tissue repair phenotype of macrophages, polarized by Th2 cytokines, activated fibroblasts through the release of TGF- β 1.²² Importantly, the upregulation of TGF- β RI and phosphorylation of SMAD2/SMAD3 in fibroblasts was also observed in the dural lesions of human HP patients, including IgG4-related HP as well as ANCA-related and idiopathic HP. These findings suggest that dural fibrosis is driven by the TGF- β 1/SMAD2/SMAD3 pathway, regardless of the baseline conditions of HP. Indeed, several lines of evidence indicate that TGF- β 1 and SMAD2/SMAD3 signaling act as master regulators of fibrosis, inducing the upregulation of collagen, fibronectin, and α -smooth muscle actin (α -SMA) in fibroblasts of multiple organs in humans and rodent models.^{23–27} We therefore suggest that the TGF- β 1/SMAD2/SMAD3 pathway might be a hitherto unknown therapeutic target for HP. In addition, TGF- β 1 facilitates the cell surface translocation of proteinase 3,^{28, 29} a major target antigen of ANCA, and the formation of neutrophil extracellular traps,^{30,31} which induce ANCA and ANCA-like disease in mice.³² Thus, TGF- β 1 may also worsen ANCA-related vasculitis and HP.

Our study is the first to demonstrate that the therapeutic administration of irbesartan *after* the inflammatory cell infiltration of the dura mater effectively ameliorates HP

and decreases multiple organ fibrosis in LATY136F mutant mice. Angiotensin II is now recognized as a growth factor that regulates cell growth and fibrogenesis by increasing the levels of TGF- β ¹³³ and connective tissue growth factors.³⁴ AT1 blockade abrogates angiotensin II-induced connective tissue growth factor, collagen type I, and α -SMA expression by a TGF- β -dependent SMAD3 signaling pathway.^{34,35} Thus, irbesartan acts as an AT1 blocker to inhibit fibroblast proliferation and collagen type I accumulation, thereby reducing tissue fibrosis. Irbesartan also modulates inflammatory responses by suppressing T cell activation.^{36,37} Consistent with this function, irbesartan inhibited the accumulation of immune cells in inflammatory lesions of the dura of LATY136F mutant mice. Thus, these dual functions of irbesartan might potentially contribute to its therapeutic effects in HP; however, in our model, the reduction in dural fibrosis was more pronounced than the inhibition of inflammatory cell infiltration. This suggests that the blockade of TGF- β and SMAD2/SMAD3 signaling is critical for the treatment of HP. Inflammation might be triggered by various causes in HP, while tissue fibrosis is a common feature in all patients with HP.^{16,38} Thus, TGF- β and SMAD2/SMAD3 blockade by AT1 blockers, such as irbesartan, may provide a novel therapeutic approach for intractable HP in humans.

The present study had some limitations. First, because the amounts of dura mater obtained from mice were very small, quantitative biochemical analyses targeted only the key molecules. Second, autopsied samples from human HP of various causes were also limited, and therefore the human results of the current study should be regarded as preliminary.

In conclusion, we developed a novel mouse model of HP in which the TGF- β 1/SMAD2/SMAD3 pathway plays a crucial role in dural inflammatory fibrosis. Because irbesartan efficiently suppressed this pathway, AT1 blockers may be a good therapeutic candidate for future clinical trials of intractable HP.

Acknowledgments

We thank Mr. Takaaki Kanemaru, Department of Morphology Core Unit, Kyushu University, for his technical assistance. We thank J. Ludovic Croxford, PhD, from Edanz Group (www.edanzediting.com/ac) for editing a draft of this manuscript. This study was supported in part by a Health and Labour Sciences Research Grant on Intractable Diseases (H26-Nanchitou (Nan)-Ippan-074) from the Ministry of Health, Labour and Welfare, Japan (J.K.); the Practical Research Project for Rare/Intractable Diseases from the Japan Agency for Medical Research and Development (AMED) (J.K.); a “Glial assembly” Grant-in-Aid for

Scientific Research on Innovative Areas (MEXT KAKENHI Grant Numbers 25117001 and 25117012) from the Ministry of Education, Culture, Sports, Science and Technology of Japan (J.K.); JSPS KAKENHI Grants-in-Aid for Scientific Research (A) (Grant Number 16H02657) (J.K.), (C) (Grant Number 16K09694) (R.Y.), and (C) (Grant Number 26461295) (K.M.) from the Japan Society for the Promotion of Science, and CNRS and INSERM (B.M. and M.M.).

Author Contributions

Y.C., K.M., and R.Y. designed and performed the experiments, analyzed the data, and wrote the manuscript; Y.H. and K.I. contributed to the preparation of LATY136F mutant mice and genotyping; S.K. provided technical assistance for the neuropathological experiment; F.H. and H.E. contributed to the MRI analysis. X.Z., T.F., H.O., S.H., T.Y., and T.M. contributed to the analysis of results; M.Y. provided autopsy specimens from patients with HP; K.Y. and M.K. contributed to the preparation of LATY136F mutant mice; M.M. and B.M. provided LATY136F mutant mice and contributed to manuscript editing; and J.K. directed the entire study, designed the experiments, and wrote the manuscript. All authors have read and approved the final version of the manuscript.

Conflicts of Interest

R.Y. has received honoraria from Biogen Japan, Bayer Schering Pharma, Novartis Pharma and Mitsubishi Tanabe Pharma; T.M. has received honoraria from Bayer Schering Pharma, Biogen Japan, Takeda Pharmaceutical Co. Ltd., and Mitsubishi Tanabe Pharma; J.K. is a consultant for Biogen Japan and Medical Review, and has received honoraria from Bayer Healthcare, Mitsubishi Tanabe Pharma, Nobelpharma, Otsuka Pharmaceutical, Sanofi K.K., Eisai, Chugai Pharmaceutical Co. Ltd., Teijin Pharma, Novartis Pharma, and Medical Review; the remaining authors declare no conflicts of interest.

References

1. Kupersmith MJ, Martin V, Heller G, et al. Idiopathic hypertrophic pachymeningitis. *Neurology* 2004;62:686–694.
2. Pai S, Welsh CT, Patel S, Rumboldt Z. Idiopathic hypertrophic spinal pachymeningitis: report of two cases with typical MR imaging findings. *AJNR Am J Neuroradiol* 2007;28:590–592.
3. Bosman T, Simonin C, Launay D, et al. Idiopathic hypertrophic cranial pachymeningitis treated by oral methotrexate: a case report and review of literature. *Rheumatol Int* 2008;28:713–718.

4. Liao B, Kamiya-Matsuoka C, Fang X, Smith RG. Refractory IgG4-related intracranial hypertrophic pachymeningitis responded to rituximab. *Neurol Neuroimmunol Neuroinflamm* 2014;1:e41.
5. Shapiro KA, Bové RM, Volpicelli ER, et al. Relapsing course of immunoglobulin G4-related pachymeningitis. *Neurology* 2012;79:604–606.
6. Yonekawa T, Murai H, Utsuki S, et al. A nationwide survey of hypertrophic pachymeningitis in Japan. *J Neurol Neurosurg Psychiatry* 2014;85:732–739.
7. Yamamoto M, Takahashi H, Shinomura Y. Mechanisms and assessment of IgG4-related disease: lessons for the rheumatologist. *Nat Rev Rheumatol* 2014;10:148–159.
8. Hamano H, Kawa S, Horiuchi A, et al. High serum IgG4 concentrations in patients with sclerosing pancreatitis. *N Engl J Med* 2001;344:732–738.
9. Stone JH, Zen Y, Deshpande V. IgG4-related disease. *N Engl J Med* 2012;366:539–551.
10. Yamada K, Zuka M, Ito K, et al. LatY136F knock-in mouse model for human IgG4-related disease. *PLoS ONE* 2018;13:e0198417.
11. Aguado E, Richelme S, Nunez-Cruz S, et al. Induction of T helper type 2 immunity by a point mutation in the LAT adaptor. *Science* 2002;296:2036–2040.
12. Genton C, Wang Y, Izui S, et al. The Th2 lymphoproliferation developing in LatY136F mutant mice triggers polyclonal B cell activation and systemic autoimmunity. *J Immunol*. 2006;177:2285–2293.
13. Sommers CL, Park CS, Lee J, et al. A LAT mutation that inhibits T cell development yet induces lymphoproliferation. *Science* 2002;296:2040–2043.
14. Riku S, Hashizume Y, Yoshida M, Riku Y. Is hypertrophic pachymeningitis a dural lesion of IgG4-related systemic disease? *Clin Neurol* 2009;49:594–596.
15. Marut W, Kavian N, Servettaz A, et al. Amelioration of systemic fibrosis in mice by angiotensin II receptor blockade. *Arthritis Rheum* 2013;65:1367–1377.
16. Lu LX, Della-Torre E, Stone JH, Clark SW. IgG4-related hypertrophic pachymeningitis: clinical features, diagnostic criteria, and treatment. *JAMA Neurol* 2014;71:785–793.
17. Jeannin P, Lecoanet S, Delneste Y, et al. IgE versus IgG4 production can be differentially regulated by IL-10. *J Immunol*. 1998;160:3555–3561.
18. Platts-Mills T, Vaughan J, Squillace S, et al. Sensitisation, asthma, and a modified Th2 response in children exposed to cat allergen: a population-based cross-sectional study. *Lancet* 2001;357:752–756.
19. Satoguina JS, Weyand E, Larbi J, Hoerauf A. T regulatory-1 cells induce IgG4 production by B cells: role of IL-10. *J Immunol*. 2005;174:4718–4726.
20. Yoshizaki A. Pathogenic roles of B lymphocytes in systemic sclerosis. *Immunol Lett* 2018;195:76–82.
21. Lech M, Anders HJ. Macrophages and fibrosis: how resident and infiltrating mononuclear phagocytes orchestrate all phases of tissue injury and repair. *Biochim Biophys Acta* 2013;1832:989–997.
22. Wynn TA, Vannella KM. Macrophages in tissue repair, regeneration, and fibrosis. *Immunity* 2016;44:450–462.
23. Cheng W, Xiao L, Ainiwaer A, et al. Molecular responses of radiation-induced liver damage in rats. *Mol Med Rep* 2015;11:2592–2600.
24. Fernandez IE, Eickelberg O. The impact of TGF-beta on lung fibrosis: from targeting to biomarkers. *Proc Am Thorac Soc* 2012;9:111–116.
25. Latella G, Vetuschi A, Sferra R, et al. Smad3 loss confers resistance to the development of trinitrobenzene sulfonic acid-induced colorectal fibrosis. *Eur J Clin Invest* 2009;39:145–156.
26. Meng XM, Nikolic-Paterson DJ, Lan HY. TGF-beta: the master regulator of fibrosis. *Nat Rev Nephrol* 2016;12:325–338.
27. Meng XM, Tang PM, Li J, Lan HY. TGF-beta/Smad signaling in renal fibrosis. *Front Physiol* 2015;6:82.
28. Csernok E, Szymkowiak CH, Mistry N, et al. Transforming growth factor-beta (TGF-beta) expression and interaction with proteinase 3 (PR3) in anti-neutrophil cytoplasmic antibody (ANCA)-associated vasculitis. *Clin Exp Immunol* 1996;105:104–111.
29. Kekow J, Csernok E, Szymkowiak C, Gross WL. Interaction of transforming growth factor beta (TGF beta) with proteinase 3. *Adv Exp Med Biol* 1997;421:307–313.
30. Alemán OR, Mora N, Cortes-Vieyra R, et al. Transforming growth factor-beta-activated kinase 1 is required for human Fc-gammaRIIb-induced neutrophil extracellular trap formation. *Front Immunol* 2016;7:277.
31. Söderberg D, Segelmark M. Neutrophil extracellular traps in ANCA-associated vasculitis. *Front Immunol* 2016;7:256.
32. Sangaletti S, Tripodo C, Chiodoni C, et al. Neutrophil extracellular traps mediate transfer of cytoplasmic neutrophil antigens to myeloid dendritic cells toward ANCA induction and associated autoimmunity. *Blood* 2012;120:3007–3018.
33. Uhal BD, Kim JK, Li X, Molina-Molina M. Angiotensin-TGF-beta 1 crosstalk in human idiopathic pulmonary fibrosis: autocrine mechanisms in myofibroblasts and macrophages. *Curr Pharm Des* 2007;13:1247–1256.
34. Yang F, Chung AC, Huang XR, Lan HY. Angiotensin II induces connective tissue growth factor and collagen I expression via transforming growth factor-beta-dependent and -independent Smad pathways: the role of Smad3. *Hypertension* 2009;54:877–884.
35. Wang W, Huang XR, Canlas E, et al. Essential role of Smad3 in angiotensin II-induced vascular fibrosis. *Circ Res* 2006;98:1032–1039.
36. Cheng SM, Yang SP, Ho LJ, et al. Irbesartan inhibits human T-lymphocyte activation through downregulation

- of activator protein-1. *Br J Pharmacol* 2004;142:933–942.
37. Dol F, Martin G, Staels B, et al. Angiotensin AT1 receptor antagonist irbesartan decreases lesion size, chemokine expression, and macrophage accumulation in apolipoprotein E-deficient mice. *J Cardiovasc Pharmacol* 2001;38:395–405.
38. Yokoseki A, Saji E, Arakawa M, et al. Hypertrophic pachymeningitis: significance of myeloperoxidase anti-neutrophil cytoplasmic antibody. *Brain* 2014;137:520–536.

Supporting Information

Additional supporting information may be found online in the Supporting Information section at the end of the article.

Figure S1. Comparison of dural lesions in wild type and LATY136F homozygous mutant mice aged 3 and 6 weeks.

Table S1. Clinical information of autopsied cases.

Table S2. Antibodies used for immunohistochemistry.

Table S3. Antibodies used for western blotting.